electronics

MDPI

Article

Research on Active Disturbance Rejection Control Technology of Electromechanical Actuators

Jing Han *, Hongfu Wang, Guotai Jiao, Liming Cui and Yuren Wang

College of Mechatronic Engineering, North University of China, Taiyuan 030051, Shanxi, China; hflovelin@sohu.com (H.W.); jiaogt@163.com (G.J.); ccuiliming@sohu.com (L.C.); wyrwqx@sohu.com (Y.W.)

* Correspondence: ajingcool@tom.com; Tel.: +86-138-3463-7620

Received: 2 August 2018; Accepted: 30 August 2018; Published: 3 September 2018

Abstract: It has been proven that the properties of non-linearity, multi-disturbance, and time-variation are the main factors affecting the performance of the electromechanical actuator (EMA) for guided artillery rockets. In particular, its controller should have good dynamic characteristics and strong anti-disturbance features when the projectile is maneuvered at the end of its guidance. For these reasons, an active disturbance rejection controller (ADRC) was designed for a guided artillery rocket's EMA with a ball screw drive. Compared to other control methods, it has been shown that the ADRC had a stronger disturbance rejection ability than PID, Fuzzy-PID, and BP-PID under the condition of 20% maximum control torque disturbance, and it also had a large stability margin and bandwidth.

Keywords: ADRC; electromechanical actuator; guided artillery rocket

1. Introduction

As one of the most important parts of the guided artillery rocket, the control system of electromechanical actuator (EMA) generates real-time instructions that drive EMA to deflect and change the flight attitude. Obviously, the control law of EMA directly affects the performance of the entire guided artillery rocket. However, due to the influence of non-linear factors such as friction, clearance, structural deformation and the load changes drastically at the end of guidance, traditional control methods can no longer meet the above requirements of modern military high-precision guidance [1]. At present, in addition to the PID control approach, there are other ways used in guided artillery rockets such as the sliding model control (SMC), H_∞ control, adaptive control, and so on. Among them, the main advantages of SMC are order reduction, decoupling design procedure, disturbance rejection, insensitivity to parameter variations and simple implementation by means of a power converter. However, it always has the chattering problem, which results from the high-frequency switching of an SMC exciting unmodelled dynamics in the closed loop [2]. The H_∞ control approach has a strong robustness and anti-disturbance ability, but only within the permissible perturbation range [3,4]. The fuzzy adaptive PID control and BP neural network adaptive PID control, as two commonly used adaptive control methods for the EMA, have effectively solved the uncertainty of the PID control parameters and environmental disturbances; it can make the system more adaptable and an anti-disturbance to the external environment. However, there are still some problems, such as the Fuzzy-PID approach finding it difficult to determine the fuzzy rules, while the BP-PID approach converges slowly and is prone to local extremum. However, the ADRC approach does not have the above problems; it has the characteristics of not relying on the model but combining it to perform the real-time estimation and subtraction of disturbances. Particularly, it has obvious advantages under vibration suppression or strong disturbance conditions, so we tried to use ADRC to control the EMA. Hongyinping Feng, et al. [5] proved mathematically that the ADRC can handle a variety of disturbances in a variety of uncertain systems. Jie Li, Yuanqing Xia, et al. [6] confirmed the truth

that the ADRC has a strong stability in the presence of parameter uncertainty. Studies [7–9] have respectively proposed ADRC control schemes for time-delay and non-linear systems. At present, ADRC has been accepted and applied more and more widely. Momir R. Stankovic, et al. [10] realized the active disturbance rejection control of the multi-axis system based on an FPGA and verified its tracking performance, stability and robustness through experiments. Bingwei Gao, Junpeng Shao, et al. [11] proposed a compound control strategy combining velocity compensation with ADRC to improve the positioning accuracy of the electro-hydraulic position servo system.

Additionally, the ADRC has been widely used in steering the controller such as automatic vehicles, the AHV model-based autopilot controller, spacecraft's attitude and position synchronization control and so on [12–17]. There was no doubting that the application on the ADRC extended to the field of the controlling missile or guided artillery rocket's EMA. Based on an improved auto-disturbance controller, Zhang Mingyue [18] proposed a method of the NSGA-II algorithm which could help to solve the ADRC parameter tuning problem. An internal and external double closed-loop auto-disturbance-rejection attitude controller design method was proposed for a certain type of missile [19]. In order to improve the trajectory tracking accuracy, an improved ADRC was built, which used the reference acceleration signal of the target trajectory as the feed forward quantity to suppress the uncompensated disturbance in the system [20]. Our paper focused on the active disturbance rejection control method for an EMA with a ball screw of a kind of guided artillery rocket, which was systematically analyzed and compared with several of the most mainstream intelligent control methods. Then the advantages of the active disturbance rejection control technology were verified. This could provide an important theoretical basis for the application of the ADRC in the guided artillery rocket.

2. System Description

2.1. Mathematical Model of the EMA

According to the working principle of EMA, we can use Equations (1)–(4) to describe its mathematical model. They represent the electromechanical conversion equation, the back EMF equation, the rotor circuit voltage equation, and the mechanical equation, respectively.

$$T_m = K_m \cdot I_A \tag{1}$$

$$E_m = K_e \cdot \omega_m \tag{2}$$

$$U_m = R \cdot I_A + L \cdot \frac{dI_A}{dt} + E_m \tag{3}$$

$$T_m = J \cdot \frac{d\omega_m}{dt} + T_f + T_h + T_\omega \tag{4}$$

After ignoring the motor armature inductance, the equations of the EMA's dynamics can be obtained by combining Equations (1)–(4).

$$\frac{d\theta}{dt^2} = \frac{U_m \cdot K_m}{R \cdot J} - \frac{T_f}{J} - \frac{T_h}{J} - \frac{T_\omega}{J} - \frac{K_e \cdot K_m}{R \cdot J} \cdot \frac{d\theta}{dt} \tag{5}$$

2.2. EMA's Active Disturbance Rejection Controller Design

In the 1980s, Han Jingqing firstly proposed the concept of active disturbance rejection control technology. The ADRC actively extracts the disturbance information from the input/output signal of the controlled object before the disturbance significantly affects the final output of the system, and then eliminates it by controlling the signal as soon as possible. In this way, it can greatly reduce its impact on the amount of control [21]. The core of the system is to sum up the unmodeled section and the unknown external disturbances of the system to estimate and compensate the "total disturbance" of

the system [22]. The non-linear ADRC is composed of an extended state observer (ESO), a tracking differentiator (TD), and a non-linear state error feedback control law (NLSEF).

According to Equation (5), we could obtain the EMA's equation of state.

$$\begin{cases} \dot{x_1} = x_2 \\ \dot{x_2} = x_3 + b \cdot U_m \\ \dot{x_3} = \dot{f} \\ y = x_1 \end{cases} \tag{6}$$

where $x_2 = \omega_m = \frac{d\theta}{dt}$, $f = -\frac{K_e \cdot K_m}{R \cdot J} \cdot x_2 - \frac{T_f}{J} - \frac{T_h}{J} - \frac{T_\omega}{J}$, $b = \frac{K_m}{R \cdot J}$, $x_1 = \theta$. U_m represents the input voltage, y represents the output angle of the motor shaft.

The ADRC observes the disturbance f by establishing an ESO and eliminates it by the NLSEF to achieve the function of anti-disturbance. Therefore, we have designed a state observer of the form of Equation (7).

$$\begin{cases} \varepsilon_1 = z_1 - y \\ \dot{z_1} = z_2 - \beta_{01} \cdot \varepsilon_1 \\ \dot{z_2} = z_3 - \beta_{02} \cdot fal(\varepsilon_1, \alpha_1, \delta) + b \cdot U_m \\ \dot{z_3} = -\beta_{03} \cdot fal(\varepsilon_1, \alpha_2, \delta) \end{cases} \tag{7}$$

According to the definition of ADRC, the discrete form of the designed controller is as follows.

- The Tracking Differentiator (TD) algorithm is given by Equation (8):

$$\begin{cases} fh = fhan(v_1(k) - v(k), v_2(k), r_0, h_0) \\ v_1(k+1) = v_1(k) + h \cdot v_2(k) \\ v_2(k+1) = v_2(k) + h \cdot fh \end{cases} \tag{8}$$

- The Extended State Observer (ESO) algorithm has the following form:

$$\begin{cases} \varepsilon_1 = z_1(k) - y(k) \\ z_1(k+1) = z_1(k) + h \cdot [z_2(k) - \beta_{01} \cdot \varepsilon_1] \\ z_2(k+1) = z_2(k) + h \cdot [z_3(k) - \beta_{02} \cdot fal(\varepsilon_1, 0.5, \delta) + b \cdot U_m] \\ z_3(k+1) = z_3(k) - h \cdot \beta_{03} \cdot fal(\varepsilon_1, 0.25, \delta) \end{cases} \tag{9}$$

- Non-linear state error feedback control law (NLSEF) algorithm is

$$\begin{cases} e_1 = v_1 - z_1, e_2 = v_2 - z_2 \\ u_0 = -fhan(e_1, c \cdot e_2, r, h_1) \\ U_m = (u_0 - z_3(k))/b_0 \end{cases} \tag{10}$$

where $v(k)$ is the input instructions of the system, $y(k)$ is the output deflection angle of the EMA, the expression of the speed synthesis function $fhan(x_1, x_2, r_0, h_0)$ is Equation (11), and the expression of the filter function fal(x, a, δ) is Equation (12).

$$\begin{cases} d = r_0 \cdot {h_0}^2, a_0 = h_0 \cdot x_2, y = x_1 + a_0 \\ a_1 = \sqrt{d \cdot (d + 8 \cdot |y|)} \\ a_2 = a_0 + sign(y) \cdot (a_1 - d)/2 \\ s_y = [sign(y + d) - sign(y - d)]/2 \\ a = (a_0 + y - a_2) \cdot s_y + a_2 \\ s_a = [sign(a + d) - sign(a - d)]/2 \\ fhan = -r \cdot \left[\frac{a}{d} + sign(a)\right] \cdot s_a - r_0 \cdot sign(a) \end{cases} \tag{11}$$

$$\text{fal(x, a, } \delta) = \begin{cases} \frac{x}{\delta^{(1-a)}}, |x| \le \delta \\ sign(x) \cdot |x|^a, |x| > \delta \end{cases} \tag{12}$$

3. ADRC Control Model for the EMA

According to Equation (5), it could be considered a second-order time-varying non-linear system with the constant change of the friction torque, hinge moment, and external disturbance in the EMA In this section, an electric canard rudder with a ball screw drive (as shown in Figure 1) was a controlled object and its control principle was shown in Figure 2. More specifically, the signal generated by the controller is sent to the driver for the aim of driving the motor. Furthermore, the output torque of the motor is continually increased by the reduction gear and the ball screw, which converts the circular motion into the linear motion of the nut. Then, the nut drives the shift fork to deflect the rudder shaft through linear displacement. At the same time, the position signal is fed back to the controller by the potentiometer. It should be specially noted that the linear potentiometer in Figure 1 measures the displacement of the screw nut, which can be converted into the deflection angle of the rudder shaft by Equation (13). Additionally, we used a rotary potentiometer in Figure 2 for convenience of illustration; it is used to measure the rudder deflection angle. The model structure of the EMA based on the ADRC was shown in Figure 3. Firstly, the ADRC generates a control instruction based on the potentiometer's feedback angle and transmits it to the driver, which amplifies the control signal to form a control voltage. Secondly, the control voltage is added to the back EMF after passing through the limiting module, which represents the range of its control voltage, then acts on the motor winding to form a current, at the same time, the electromechanical conversion is performed to form a torque. Thirdly, the torque is added to the motor output shaft by the friction torque and the disturbance torque, it is converted into angular acceleration by the mechanical equation. After two integrations, the output angle of the motor shaft is obtained. Furthermore, it is multiplied by the total deceleration to become the rudder deflection radians, which needs to be converted to an angle, finally. The friction torque equation and the hinge torque equation are as shown in Equations (14) and (15). The driver's transfer function is Equation (16).

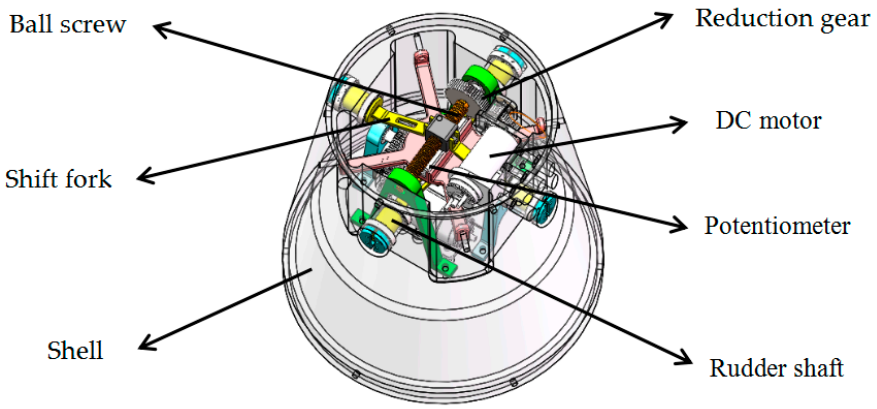

Figure 1. The prototype of EMA.

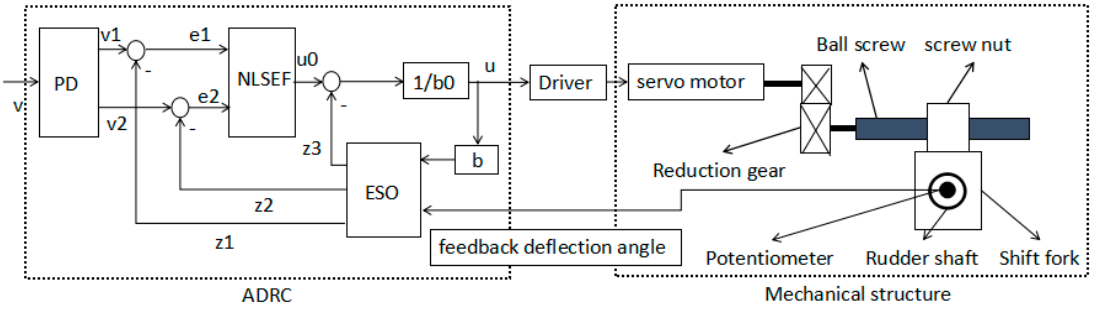

Figure 2. The schematic diagram of EMA with ball screw based on ADRC.

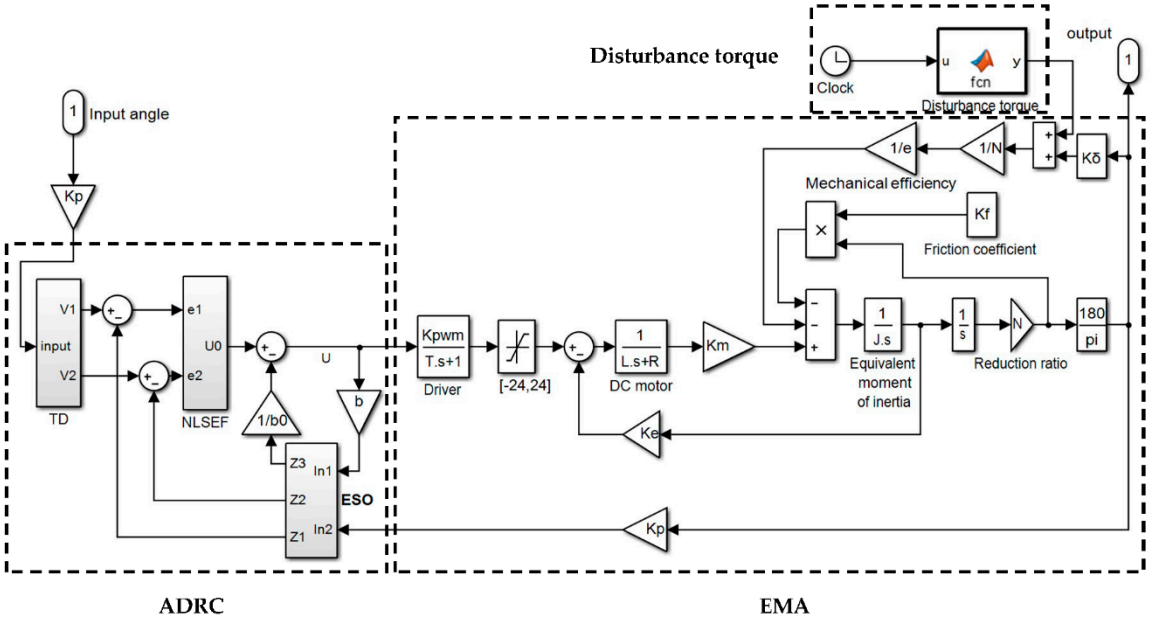

Figure 3. The ADRC control model Schematic of EMA.

Conversion equation of screw nut displacement and rudder deflection angle

$$\theta = arctan\frac{x}{L} \tag{13}$$

$$T_f = K_f \cdot \theta \cdot \frac{\pi}{180^\circ} \tag{14}$$

$$T_h = \frac{K_\delta \cdot \theta}{N} \tag{15}$$

$$G_D(S) = \frac{K_{PWM}}{T \cdot s + 1} \tag{16}$$

where $K_{PWM} = \frac{U_S}{U_C}$, $T = \frac{1}{f_{pwm}}$.

In our paper, the ADRC adopted the dynamic parameter adjustment method [21] (pp. 58–59) to adjust the control parameters. In this way, TD, ESO, and NLSEF are regarded as mutually independent three parts. In the TD part, the input signal $v0$ is followed by $v1$ and the differential signal of the input signal $v0$ is followed by $v2$. Moreover, the h is the simulation step size and the $h0$ could be an integer multiple of it. In addition, the TD's tracking speed is determined by r. In regard to the ESO, the three outputs of which are $z1$, $z2$, and $z3$. The $v1$, $v2$ is tracked by $z1$, $z2$ and the disturbance volume is tracked by $z3$ almost simultaneously. For a servo system with such large inertia and large time lag, β_{01}, β_{02} and β_{03} should also be correspondingly large. According to its empirical method with the Fibonacci sequence, we can make $\beta_{01} = \frac{1}{h}$, $\beta_{02} = \frac{1}{3h^2}$, $\beta_{03} = \frac{1}{8^2h^3}$. Normally, the linear interval δ is generally desirable from $5\,h$ to $10\,h$, besides the control accuracy of the NLSEF is affected by the $h1$. Additionally, the rapid response of the ADRC control system is influenced by the damping coefficient c. The response speed of the system is also affected by the control gain r which needs to be adjusted according to specific conditions.

In the structure of the EMA, a Maxon DCX26L GB KL 24 V was used as the servo motor. The motor's parameters and ADRC's parameters, which were used in the model, are shown in Table 1. The data in the table were brought into Figure 3 to obtain the ADRC simulation model of the EMA, as shown in Figure 4, where the b01, b02, and b03 represent the β_{01}, β_{02}, and β_{03} respectively.

Table 1. The servo system's parameters.

Parameter/Symbol	Value/Unit	ADRC's Parameters	Value
Terminal resistance (R)	0.74 Ohm	TD Integral step (h0)	0.001
Terminal Inductance (L)	0.129 mH	TD Tracking speed factor (r0)	12.0000
Torque constant (K_m)	21.4 mN·m/A	NLSEF Integral step (h1)	0.001
Speed constant (K_e)	445 rpm/v	Control quantity replenishment factor (r)	200
Equivalent load moment of inertia (J)	31.35 g·cm^2	Damping factor (c)	1.2
Total reduction ratio (N)	277.776	Compensation factor (b0)	150
Potentiometer conversion factor (K_P)	0.086 V/°	β_{01}	1000
Drive magnification (K_{PWM})	7.3	β_{02}	33.3333
Drive time constant (T)	10^{-4}s	β_{03}	3125.0000
Hinge torque load factor (K_δ)	0.667 N·m/°	Linear interval (delta)	0.005
Frictional moment factor (K_f)	1.154 N·m/rad	Simulation step (h)	0.001

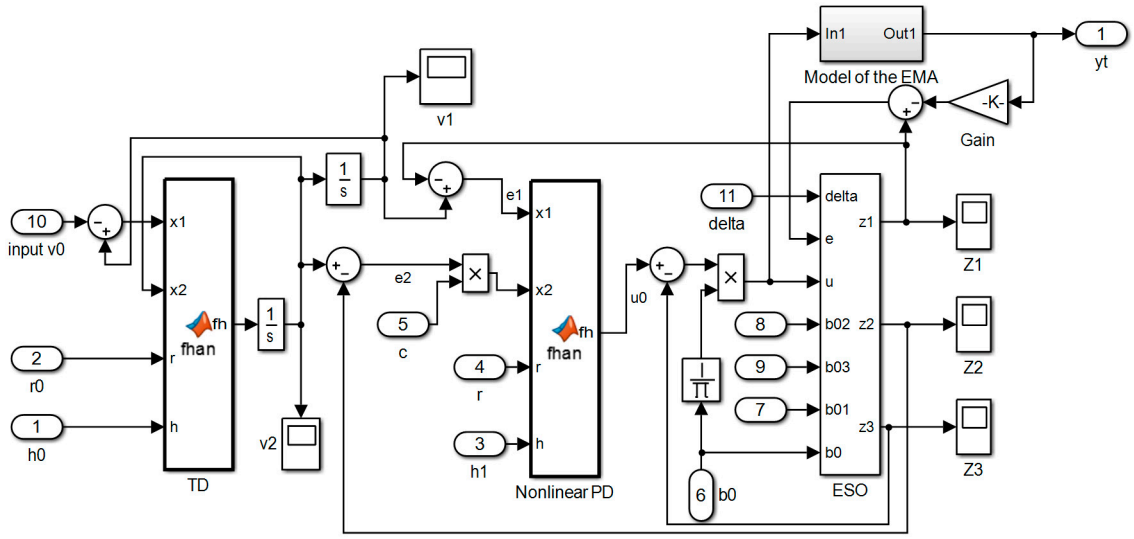

Figure 4. The ADRC simulation model of EMA.

4. Anti-Disturbance Analysis of ADRC for EMA

Many uncertain factors are inevitable during the flight of missiles and these random disturbance factors have a decisive influence on its own movement, the stability, and the final hit accuracy [23]. In the theory of ADRC, the unmodeled parts of the system and the unknown disturbances should be regarded as total disturbances. The ESO is used as a way to estimate the total disturbances in real time and eliminate them.

The fin of the guided artillery rocket or missile would be subjected to great aerodynamic loads when it is flying in the air, and that is often referred to as a hinge torque. The hinge torque acts as the main load torque of the servo, and the working performance of the servo will be affected by its wide-range changes which even destroy its movement law sometimes. When the fin of the EMA is disturbed by gusts or the projectile is maneuvered at the end of the guidance, the missile will be disturbed by the load. According to the length of the action, the disturbance received by the missile is divided into frequent disturbance and instantaneous disturbance; frequent disturbance such as friction, and instantaneous disturbance such as gust. It should be emphasized that in this paper, two non-linear factors, gust disturbance, and friction, are mainly considered. The friction mainly manifests as viscous friction acting in the system without interruption, while the gust disturbance can be reflected by the torque acting on the fin of EMA [24]. Zhiqiang Gao, Shaohua Hu, et al. [25] use 20% of the maximum control torque of the servo as disturbance torque to study the Anti-disturbance performance of the controller. Therefore, we used a similar method to apply disturbance because the maximum control torque of this type of rocket is about 10 N·m in each channel, so we use the moment disturbance which

is 2 N·m with a duration of 0.1 s as the disturbance model (as shown in Figure 5). Then we compare it with a well-tuned PID controller, fuzzy adaptive PID controller [26] and BP-PID (3-5-3 structure) controller [27] to study the EMA's anti-disturbance.

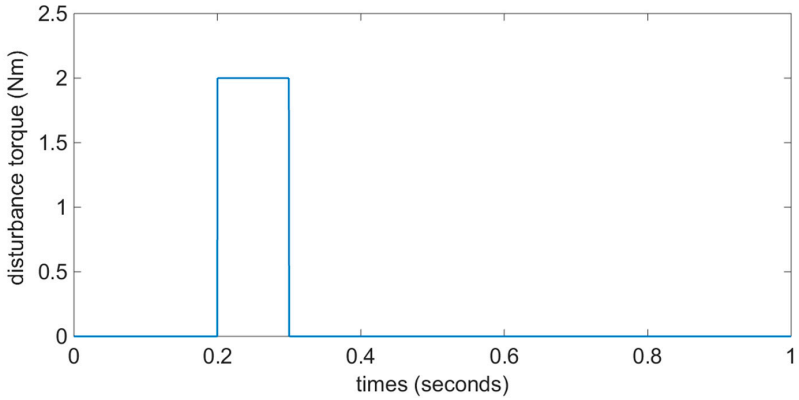

Figure 5. The disturbance model.

4.1. Time Domain Performance Analysis

Under the elastic load condition which was replaced by a hinge torque, each controller responded to a command of 1 degree in 0.5 s. At the same time, we applied 20% of the maximum control torque (2 N·m) as a load disturbance in the fin position of the model within 0.2 to 0.3 s to study the anti-disturbance of each controller. The observed and tracked situation of disturbances by the ADRC was shown in Figure 6a. It could be seen that the torque disturbances applied between 0.2 and 0.3 s were well tracked by the ESO. As shown in Figure 6b, the control torque was adjusted by the ADRC to compensate for the disturbance. Furthermore, the responses of each control model to the command and disturbance were shown in Figure 7, which reflected the response of the system without disturbance in the first 0.2 s. We could find that the rise time of ADRC was 0.05 s, however, that of the other controllers were between 0.055 and 0.08 s. Apart from this, the ADRC's overshoot was almost zero, while that of the other controllers were between 0.5 and 2.4 percent. As Figure 7 showed that the ADRC controller was only experienced in the appearance and disappearance of the disturbance, it is attributed to the compensation mechanism of ADRC, in which the sudden appearance and disappearance of the interference are both regarded as 'disturbances' for the ADRC. More specifically, the maximum disturbance of ADRC was 0.002 degrees, whereas that of the others were between 0.012 and 0.024 degrees. When the disturbance disappeared from 0.3 to 0.5 s, only the ADRC could keep the system's steady-state error at zero, however, the other controllers could only keep it between 0.004 and 0.013 degrees. In addition, the quantified time domain indexes were filled in Table 2.

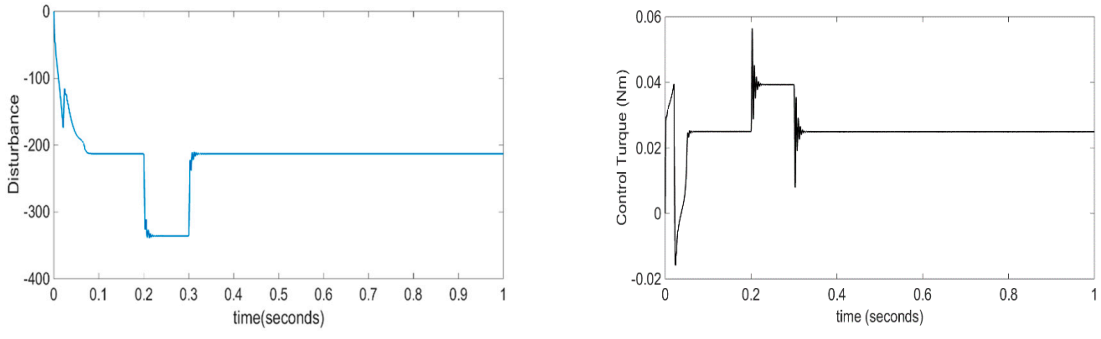

(**a**) (**b**)

Figure 6. The observational tracking of disturbances by extended state observer (ESO); (**a**) Observations of disturbance; (**b**) The control torque generated by the ADRC based on the disturbance.

Table 2. The performance of each control model under the 2 N·m moment disturbance.

Index / Controller	Rise Time (s)	Overshoot (%)	Maximum Disturbance (deg)	Steady-State Error (deg)
PID	0.08	0.5	0.024	0.0042
Fuzzy-PID	0.07	0.4	0.012	0.0125
BP-PID	0.055	2.4	0.02	0.006
ADRC	0.05	0	±0.002	0

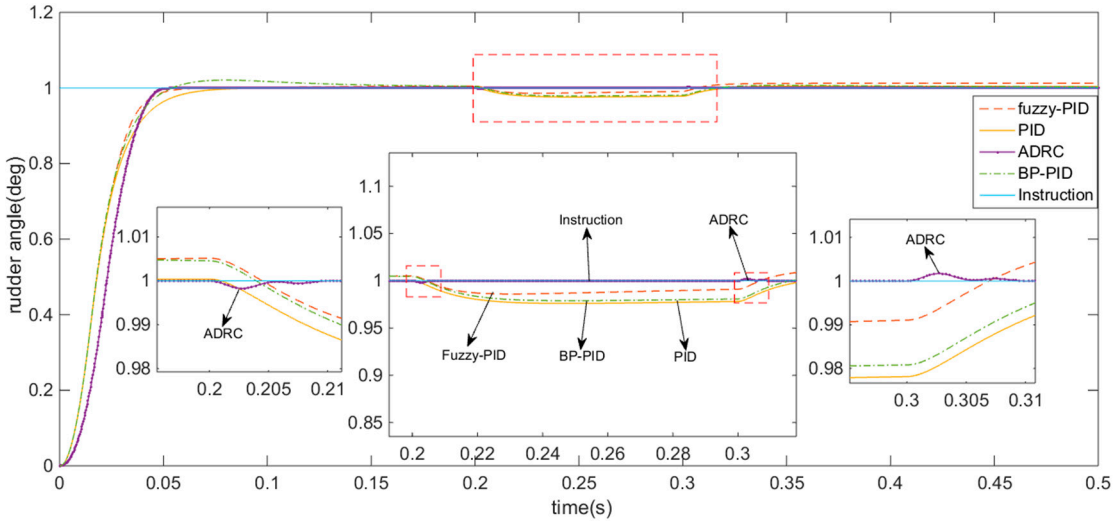

Figure 7. The comparison of step response and disturbance to each control model.

Each control model was used to track and respond to a sine command with the frequency of 1 Hz and the amplitude of 1 degree in 1 s. Similarly, we also imposed a 2 N·m of torque disturbance between 0.2 and 0.3 s. The Response conditions were shown in Figure 8. It is obvious that the tracking of ADRC has not been significantly affected, while that of the other controllers has obvious disturbance responses at the peak, where the largest amplitude deviation is about 0.05 degrees. Although the anti-disturbance of the Fuzzy-PID controller and the BP-PID controller are slightly better than that of the ordinary PID controller, the overall effect is not obvious. In the second half of each cycle, it could be seen that the ADRC has the smallest amplitude error in the command tracking.

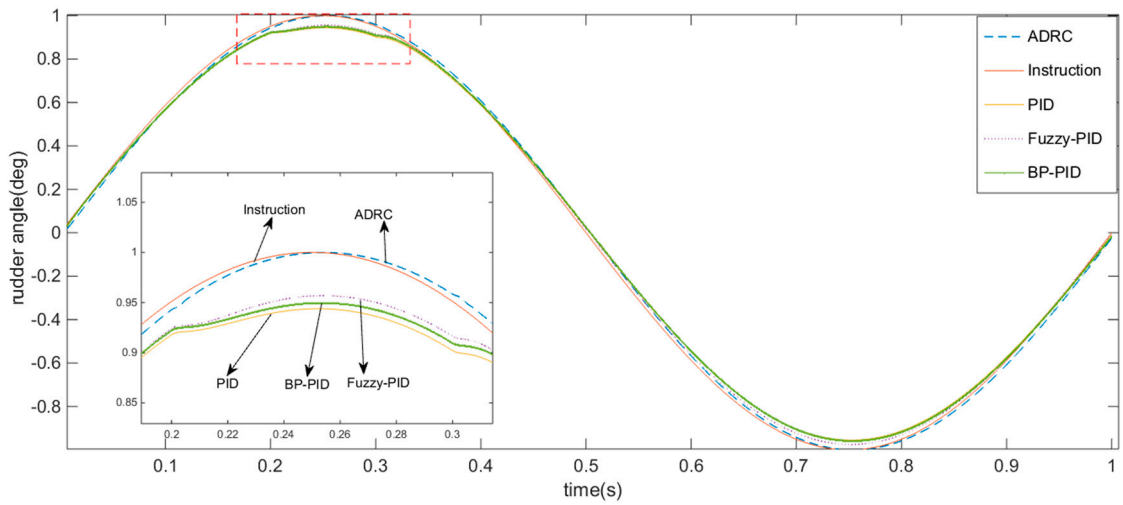

Figure 8. The anti-disturbance performance of the sinusoidal instruction tracking for each control model.

4.2. Frequency Domain Performance Analysis

In the case of the 2 N·m moment disturbance, the open-loop bode diagram for each control model was shown in Figure 9, and the closed-loop bode diagram was shown in Figure 10. According to the former, we could find that the amplitude margin of the ADRC control model was 61.6 dB, while that of the other three control models were between 24.8 and 50.2 dB. Furthermore, the phase margin of the ADRC control model was 87.8 degrees, but that of the other control models were between 18.5 and 62.3 degrees. In addition, the phase margin and amplitude margin of the Fuzzy-PID control model and the BP-PID's were almost the same, which showed the similar frequency characteristics at this frequency band. From the closed-loop bode diagram, we could see that the −3 dB bandwidth of the ADRC model was 67.1 Hz, moreover, the Fuzzy-PID's and the BP-PID's were both 46 Hz, and the PID's was 102 Hz. The quantified frequency domain indicators are filled in Table 3. So, we believe that the ADRC had a better instruction tracking performance than the other two methods, and a stronger high-frequency signal suppression capability than the PID controller. These high-frequency signals were generally considered as "noise", compared with the other two control models, ADRC had a weaker suppression of high-frequency signals in the range of 0~2000 Hz, while having the highest suppression ability of high-frequency signals in the range of 2000 Hz or above. Simultaneously, we could also find that the Fuzzy-PID control model and the BP-PID's resonated when the frequency was around 30 Hz.

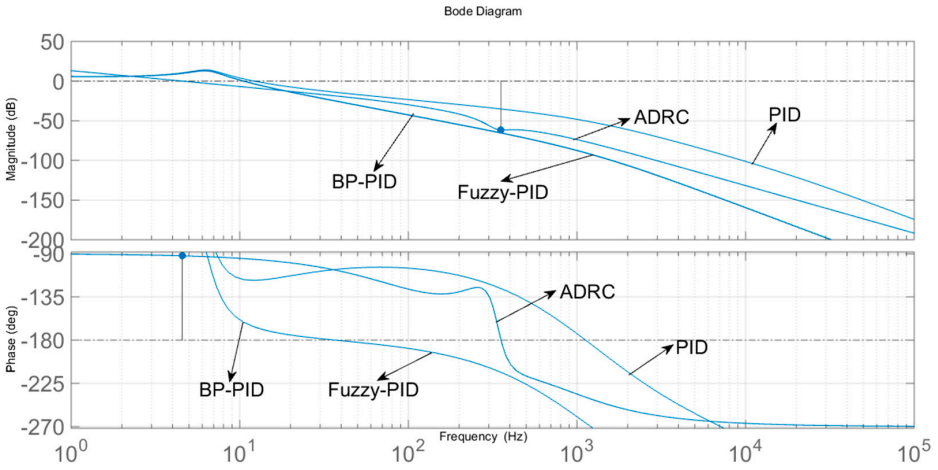

Figure 9. The open-loop bode diagram of each control model under a 2 N·m moment disturbance.

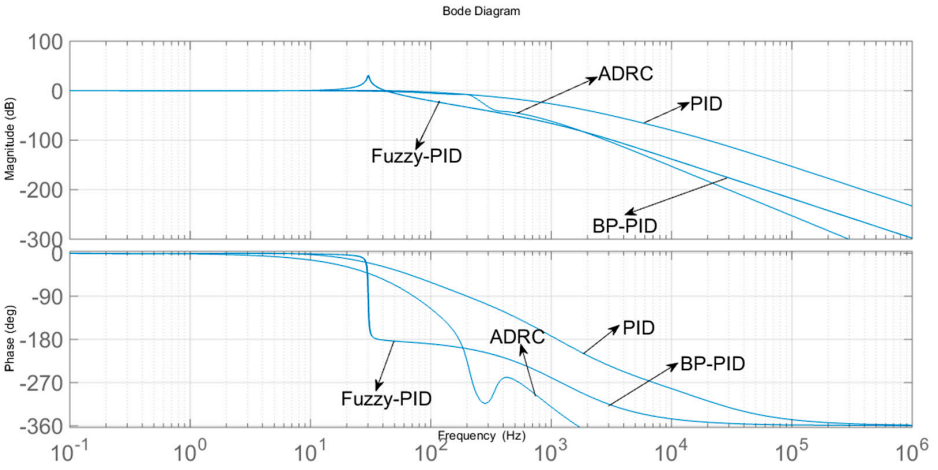

Figure 10. The closed-loop bode diagram of each control model under a 2 N·m moment disturbance.

Table 3. The stability margins and bandwidth of each control model under a 2 N·m moment disturbance.

Index \ Controller	PID	ADRC	Fuzzy-PID	BP-PID
Amplitude margin (dB)	50.2	61.6	24.8	25.2
Phase margin (deg)	62.3	87.8	18.5	19.2
Bandwidth (Hz)	102	67.1	46	46

The closed-loop zero-pole distribution map of the ADRC control model under a 2 N·m torque disturbance was shown in Figure 11. The poles are -10.1, -3.750 ± 459i, -0.1921 ± 3i, -0.786, -0.5, -0.319. It obvious that this system does not have poles in the right half-plane, so it is stable without any doubt.

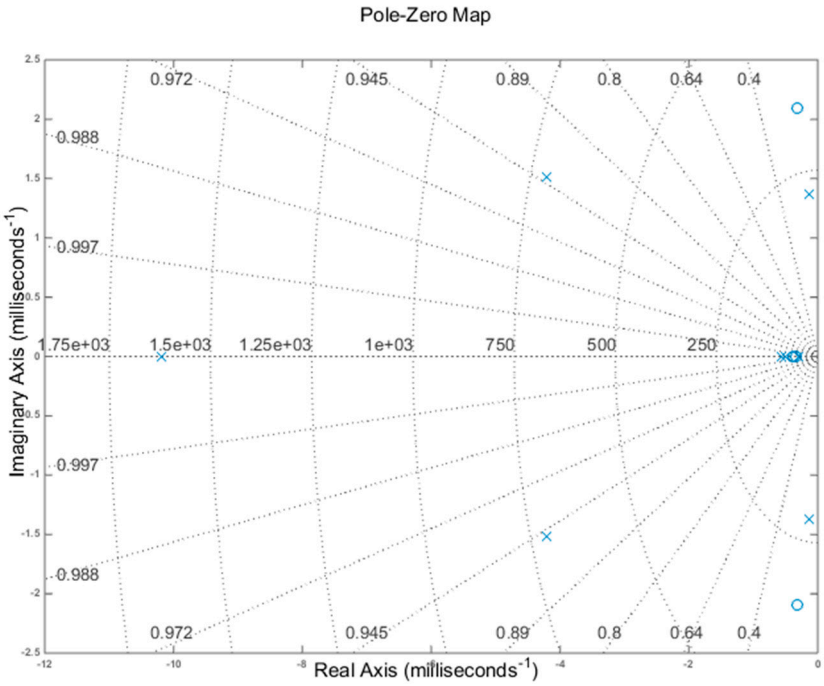

Figure 11. The closed-loop zero-pole distribution of the ADRC control model under a 2 N·m moment disturbance.

5. Conclusions

The ADRC control model was established for the guided artillery rocket's electric canard rudder with a ball screw drive. The ADRC's anti-disturbance performance was systematically analyzed by comparison with the PID's, the Fuzzy-PID's, and the BP-PID's. So, the following conclusions were drawn:

(1) Comparing with the traditional PID control model, the Fuzzy-PID's and the BP-PID's, the ADRC control model has made the response faster and the overshoot less, while it has a smaller steady-state error and stronger anti-disturb ability.

(2) In the frequency domain, the ADRC control model has superiorities with a large stability margin, a large bandwidth, and a strong high-frequency signal suppression capability. That means that the system could still remain stable under certain disturbance conditions.

(3) Although the Fuzzy-PID controller and the BP-PID controller enhanced the adaptability of the controller through the real-time adjustment of parameters, it did not essentially solve the disadvantages caused by the way of eliminating the error of the PID controller. As a

result, the anti-disturbance of the controllers was not really improved. However, ADRC could solve the contradiction between "fastness" and "overshoot" through TD. It also observed the "unknown disturbance" in real time through the ESO and makes compensations. Therefore, its anti-disturbance performance is superior. Of course, the tuning of non-linear ADRC is a complex process. The constraints between the parameters are not clear enough and the relevant empirical formulas do not have a universal guiding significance. Therefore, it is difficult to find the optimal parameters of ADRC, furthermore, it also puts higher requirements on the MCU due to the calculation of so many parameters.

Author Contributions: Conceptualization, H.J. and J.G.; Methodology, H.J.; Validation, W.H., C.L. and W.Y.; Formal Analysis, W.H.

Acknowledgments: This research is financially supported by the China Postdoctoral Science Foundation (2015 **M**571289).

Conflicts of Interest: The authors declare no conflict of interest.

Symbolic Abbreviated

Representative Meaning	Symbols	Representative Meaning	Symbols
Motor torque	T_m	Total friction torque converted to the motor shaft	T_f
Torque constant	K_m	The hinge torque that is converted to the motor shaft	T_h
Armature current	I_A	Disturbing torque that is converted to the motor shaft	T_ω
Back electromotor force	E_m	Displacement of screw nut	x
Speed constant	K_e	Vertical distance from the screw axis to the center of the rudder shaft	L
Rotor angular velocity	ω_m	Frictional moment factor	K_f
Input voltage across the motor	U_m	Hinge torque load factor	K_δ
Terminal resistance	R	Total reduction ratio	N
Terminal Inductance	L	Drive magnification	K_{PWM}
Equivalent load moment of inertia	J	Working power supply voltage	U_S
Rudder deflection angle	θ	Input voltage of PWM controller	U_C
Potentiometer conversion factor	K_P	Drive time constant	T
Representative Meaning	**Acronyms**	**Representative Meaning**	**Acronyms**
Active Disturbance Rejection Controller	ADRC	BP neural network adaptive PID	BP-PID
Electromechanical Actuator	EMA	Extended state observer	ESO
Proportion-integral-derivative	PID	Tracking differentiator	TD
Fuzzy adaptive PID	Fuzzy-PID	Non-linear state error feedback	NLSEF

References

1. Wang, Z. Fuzzy PID Control in Electric Steering Engine for Nonlinear Factor. Master's Thesis, University of Chinese Academy of Sciences, Changchun, China, 2015. (In Chinese)
2. Panchade, V.M.; Chile, R.H.; Patre, B.M. A survey on sliding mode control strategies for induction motors. *Annu. Rev. Control* **2013**, *37*, 289–307. [CrossRef]
3. Ren, Y.; Wang, W.; Wang, Y. Incremental H_∞ control for switched nonlinear systems. *Appl. Math. Comput.* **2018**, *331*, 251–263. [CrossRef]
4. Monneta, D.; Ninin, J.; Clement, B. A global optimization approach to H_∞ synthesis with parametric uncertainties applied to AUV control. *IFAC-PapersOnLine* **2017**, *50*, 3953–3958. [CrossRef]

5. Feng, H.; Guo, B. Active disturbance rejection control: Old and New results. *Annu. Rev. Control* **2017**, *44*, 238–248. [CrossRef]
6. Li, J.; Xia, Y.; Qi, X.; Zhao, P. Robust absolute stability analysis for interval nonlinear active disturbance rejection based control system. *ISA Trans.* **2017**, *69*, 122–130. [CrossRef] [PubMed]
7. Hao, S.; Liu, T.; Wang, Q. Enhanced active disturbance rejection control for time-delay systems. *IFAC-PapersOnLine* **2017**, *50*, 7541–7546. [CrossRef]
8. Wu, Z.; Guo, B. Approximate decoupling and output tracking for MIMO nonlinear systems with mismatched uncertainties via ADRC approach. *J. Frankl. Inst.* **2018**, *355*, 3873–3894. [CrossRef]
9. Fu, C.; Tan, W. Control of unstable processes with time delays via ADRC. *ISA Trans.* **2017**, *71*, 530–541. [CrossRef] [PubMed]
10. Stankovic, M.R.; Manojlovic, S.M.; Simić, S.M.; Mitrović, S.T.; Naumović, M.B. FPGA system-level based design of multi-axis ADRC controller. *Mechatronics* **2016**, *40*, 146–155. [CrossRef]
11. Gao, B.; Shao, J.; Yang, X. A compound control strategy combining velocity compensation with ADRC of electro-hydraulic position servo control system. *ISA Trans.* **2014**, *53*, 1910–1918. [CrossRef] [PubMed]
12. Chu, Z.; Sun, Y.; Wu, C.; Sepehri, N. Active disturbance rejection control applied to automated steering for lane keeping in autonomous vehicles. *Control Eng. Pract.* **2018**, *74*, 13–21. [CrossRef]
13. Tian, J.; Zhang, S.; Zhang, Y.; Li, T. Active disturbance rejection control based robust output feedback autopilot design for airbreathing hypersonic vehicles. *ISA Trans.* **2018**, *74*, 45–59. [CrossRef] [PubMed]
14. Gao, C.; Yuan, J.; Zhao, Y. ADRC for spacecraft attitude and position synchronization in libration point orbits. *Acta Astronaut.* **2018**, *145*, 238–249. [CrossRef]
15. Huang, Z.; Liu, Y.; Zheng, H.; Wang, S.; Ma, J.; Liu, Y. A self-searching optimal ADRC for the pitch angle control of an underwater thermal glider in the vertical plane motion. *Ocean Eng.* **2018**, *159*, 98–111. [CrossRef]
16. Balajiwale, S.; Arya, H.; Joshi, A. Study of performance of ADRC for longitudinal control of MAV. *IFAC-PapersOnLine* **2016**, *49*, 585–590. [CrossRef]
17. Zhang, Y.; Cao, B.; Kang, L.; Xu, J. Controller design for small wind generator with ADRC. *Procedia Environ. Sci.* **2011**, *11*, 1128–1134.
18. Zhang, M. Nonlinear Analysis and Control of EMA with Ball Screw Drive. Ph.D. Thesis, University of Chinese Academy of Sciences, Changchun, China, 2014. (In Chinese)
19. Chen, X.; Yang, D.; Geng, B. Application of Auto-Disturbance-Rejection-Controller to a Missile. *Flight Dyn.* **2006**, *24*, 81–84. (In Chinese)
20. Cui, Y. Research on Rolling Control Technology of Guided Artillery Rocket's Fixed Canard Rudder. Ph.D. Thesis, Nanjing University of Science & Technology, Nanjing, China, 2014. (In Chinese)
21. Zhu, B. *Introduction to Active Disturbance Control*; Beijing University of Aeronautics and Astronautics Press: Beijing, China, 2017; pp. 19–59. ISBN 978-7-5124-2383-1. (In Chinese)
22. Han, J. From PID to active disturbance rejection control. *IEEE Trans. Ind. Electron.* **2009**, *56*, 900–906. [CrossRef]
23. Yang, C. The Stability of Projectile under Stochastic Disturbance. Master's Thesis, Nanjing University of Science & Technology, Nanjing, China, 2016. (In Chinese)
24. Han, Z. *Exterior Ballistics of Projectiles and Rockets*; Beijing Institute of Technology Press: Beijing, China, 2014; p. 506. ISBN 978-7-5640-8709-8. (In Chinese)
25. Gao, Z.; Hu, S.; Jiang, F. A novel motion control design approach based on active disturbance rejection. In Proceedings of the Conference on Decision and Control, Orlando, FL, USA, 24–27 December 2001; Volume 40, pp. 4877–4882.
26. Hou, X. Design of the Steering Engine Control System for Missiles Based on DSP. Master's Thesis, Xidian University, Xi'an, China, 2008. (In Chinese)
27. Liu, S. Research on Neural Network Control System of Hybrid Stepping Motor. Master's Thesis, Zhejiang University, Hangzhou, China, 2013. (In Chinese)